A nonlinear beam-spring-beam element for modelling the flexural behaviour of a timber-concrete sandwich panel with a cellular core

Citation for published version:
Ou, Y, Fernando, ND, Sriharan, J, Gattas, JM & Zhang, S 2021, 'A nonlinear beam-spring-beam element for modelling the flexural behaviour of a timber-concrete sandwich panel with a cellular core', *Engineering Structures*, vol. 244, 112785. https://doi.org/10.1016/j.engstruct.2021.112785

Digital Object Identifier (DOI):
10.1016/j.engstruct.2021.112785

Link:
Link to publication record in Edinburgh Research Explorer

Document Version:
Peer reviewed version

Published In:
Engineering Structures

A nonlinear beam-spring-beam element for modelling the flexural behaviour of a timber-concrete sandwich panel with a cellular core

Ou Ya[a], Dilum Fernando[b,*], Jasotharan Sriharan[c], Joseph M. Gattas[c], Shishun Zhang[d]

[a] School of Civil Engineering, Central South University of Forestry and Technology, Changsha 410004, China

[b] School of Engineering, University of Edinburgh, Edinburgh, EH9 3FB, Scotland, UK

[c] School of Civil Engineering, University of Queensland, St Lucia 4072 Australia

[d] School of Civil and Hydraulic Engineering, Huazhong University of Science and Technology, Wuhan 430074 China

[*] Corresponding author. *E-mail address:* dilum.fernando@ed.ac.uk (D. Fernando)

Abstract

Timber-concrete composite panels are commonly used as a sustainable alternative for reinforced concrete floor construction systems. Their performance also continues to advance with new approaches to interfacial shear connection and layer composition, for example as three-layer sandwich panels with a concrete compressive face layer, timber tensile face layer, and a cellular core. Due to significant difference in stiffness of the layers, such sandwich panels demonstrate large transverse shear deformations when subjected to bending. Existing finite element modelling techniques, relying on traditional shell or solid elements, can become computationally expensive when simulating the behaviour of sandwich panels. This paper presents a new composite element for simplified numerical modelling of sandwich panels, greatly reducing the computational effort. The proposed element comprises two face layers connected by an interlayer, with face layers considered as beams and the interlayer considered as springs. A numerical model was developed using the proposed element and was validated

against finite element results of linear sandwich beams and experimental results of nonlinear, cellular-cored timber-concrete sandwich panels.

Keywords: Timber-concrete composite panels, sandwich panels, flexural behaviour, composite element, finite element modelling.

1. Introduction

Timber-concrete composite panels have become increasingly popular within the construction industry as a sustainable and lightweight alternative for reinforced concrete floor panels [1]. In timber-concrete composite panels, concrete is used as the compression element and timber is used pre-dominantly to carry the tensile loads [1, 2]. The performance of such composite panels depends significantly on the interfacial shear force transfer between concrete and timber. The concrete and timber layers are usually connected through metal mechanical shear connectors [3-5], notches in the timber [6-8], or adhesive bonding [9-11]. In many of the investigated configurations, concrete beside the bi-material interface acts in tension and thus contributes little towards the load carrying capacity of the panel. Attempts have been made to reduce the weight of the timber-concrete composite panels by introducing a lightweight interlayer, also referred to as a "core", between the concrete and timber [12, 13], thus transforming the composite panel into a sandwich panel system. The interlayer of sandwich panels can be a solid, a porous foam or a cellular structure [14-19]. Considering the similarity of the composite floor panels with an interlayer and sandwich panels in flexural behaviour, both structural systems are called "sandwich panels" hereafter.

A recent study on timber-concrete floor panels with a cellular core structure subjected to flexural loading showed significant transverse shear deformations between concrete and timber layers [13]. Similar behaviour was also commonly observed in other sandwich structures, especially those with an interlayer with a low stiffness [15, 16, 19]. In addition, such panels also show a clear change in the strain distribution gradient across the thickness of the panel at the face panel-core interface. Therefore, the behaviour of sandwich panels with a soft interlayer cannot be modelled using classical Euler-Bernoulli or Timoshenko beam theories [20-24].

Many numerical approaches have been developed for modelling of sandwich panels [25-33], with different approaches pursued for representation of the interlayer behaviour. The most common approaches are those that utilise contact or interface elements and those that utilise solid elements [25-31]. Some few studies assumed a perfect bond/composite action between the faces [34], however such assumption is not valid for most timber-concrete sandwich panels and thus those approaches are not discussed further in this paper.

When contact elements or interface elements are used to model the behaviour of interlayer, the constitutive law of these elements under mode II (and often also under mode I) loading should be known first [35]. Such constitutive laws are often obtained experimentally [35, 36]. Many interface elements have adopted traction-separation laws to characterize the behaviour of the interlayer [37] and have been used successfully in predicting the behaviour of sandwich panels. The use of solid elements to model the interlayer behaviour eliminates the need to obtain the interlayer behaviour experimentally, and only the material properties are needed instead. The use of solid elements, however, involves more computational efforts than using contact or interface elements, due to the large number of elements required to accurately capture the nonlinear behaviour of the interlayer [38, 39].

While the above numerical modelling approaches can accurately predict the flexural behaviour of sandwich panels, such approaches require significant computational efforts. Thus, they are not often considered as suitable for design use.

Against this background, this paper presents a simplified numerical modelling approach to accurately capture the nonlinear behaviour of sandwich panels. A new three-layer element is proposed to simulate the sandwich beam. The face panels are modelled as Euler-Bernoulli beams, while the interlayer is modelled as interlayer springs. The stiffness matrix of this new element is presented in Section 2; a solution procedure to consider the nonlinear behaviour through stiffness update, thus to predict the nonlinear load-displacement behaviour of the sandwich panels until ultimate load is presented in Section 3; and finally, the model is validated against existing experimental results on timber-concrete floor panels with a cellular interlayer in Section 4. The proposed model can be programmed using a simple programming language such as MATLAB [40] or Python [41], thus can be used with little effort by practitioners.

2. Structural model and formulation

While the timber-concrete sandwich panel system can be used as either one-way slab or two-way slab, the present study will be only focused on one-way slab configuration, which will potentially be the predominant application scenario of such panel system. The one-way timber-concrete sandwich panel can be treated as a beam. In developing the composite element, the sandwich panel is simplified as a three-layer system, as shown in Fig. 1. The face layers *a* and *b* represent the concrete and timber panels of the timber-concrete sandwich panel system respectively, and the interlayer *c* between them is to be modelled using spring elements. The elastic modulus, cross-sectional area, and second moment of area of the two face layers are denoted by E^n, A^n, and I^n respectively, where the superscript *n* takes the value either *a* or *b*. The shear stiffness and normal stiffness of the interlayer *c* are denoted by K_s and K_n respectively. The height of the layers *a*, *b*, and *c* are denoted by h^a, h^b, and h^c respectively. The distance between the centroids of the upper and lower face layers to the centroid of the interlayer are denoted by C^a and C^b respectively. The segment is considered to be subjected to a distributed load $q(x)$ as shown in Fig. 1.

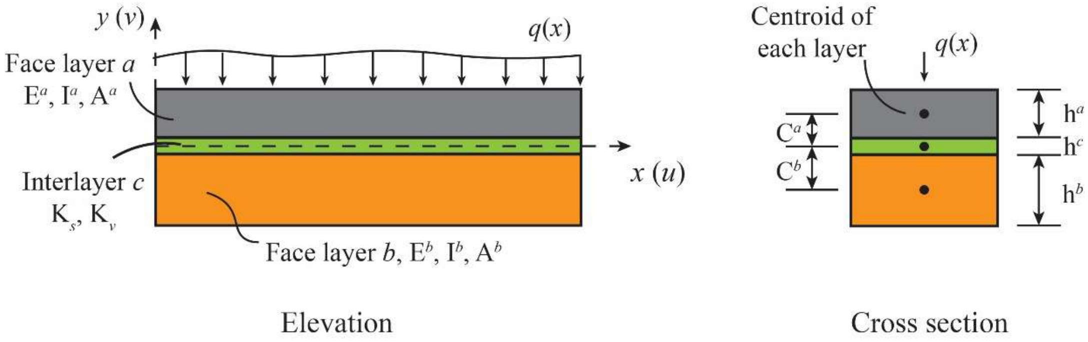

Fig. 1 Simplified three-layer system of the sandwich panel.

In the development of the composite element, the following assumptions are made:

(a) The deformation is small compared to the span of the structure;

(b) The cross section of each face layer is constant along the length;

(c) The transverse shear deformation of the face layers can be ignored and thus each face layer in the developed element can be modelled using a Euler-Bernoulli beam element;

(d) The panel system is incompressible along its thickness direction, i.e. the relative vertical deformation between face layers *a* and *b* is negligible. This implies that in the interlayer, the vertical stiffness K_n is much larger than the shear stiffness K_s.

A deformed segment of the panel is shown in Fig. 2. The nodes introduced at the ends of both face layers have three degrees of freedom: the deformation along x-axis u, the deformation along y-axis v, and the rotation θ. According to assumptions (a), (c), and (d), the relative slip γ_i between face layers *a* and *b* can be calculated from:

$$\gamma_i = u_i^a - u_i^b + \theta_i (C^a + C^b) = u_i^a - u_i^b + \theta_i^a C^a + \theta_i^b C^b \qquad (1)$$

where u_i^n ($n = a, b$) is the nodal transformation of the face layer *a* or *b* along x-axis; and θ_i is the rotation of the cross section, according to assumption (d), $\theta_i^a = \theta_i^b = \theta_i$ at the same cross section.

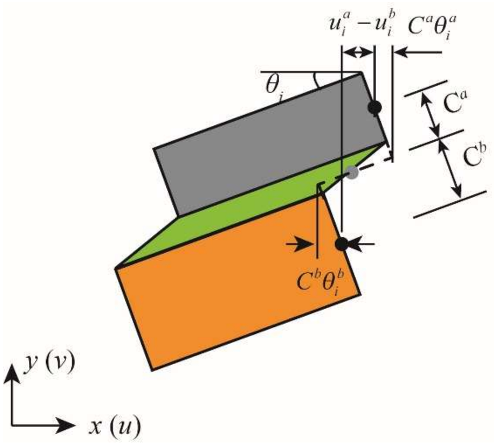

Fig. 2 Geometric relationship between transformation, rotation, and slip.

Fig. 3a shows the idealization of a panel segment in the proposed composite element. In this element, each of the face layers is modelled using a two-node beam, and the interlayer is modelled using two springs (a shear spring and a normal spring) at each element end. Fig. 3b illustrates the force components in a deformed element, with load transfer assumed only to occur at element nodes. Interfacial forces are transferred by the springs at each element node: a shear force F_{ui} from the shear spring, and a normal force F_{vi} from the normal spring. Subscripts 1 and 2 represent the two ends of the element as shown in Fig. 3b. For nodal axial force N_i^j, shear force V_i^j, and bending moment M_i^j, superscripts *a* and *b* are additionally used to represent the top and bottom face layers.

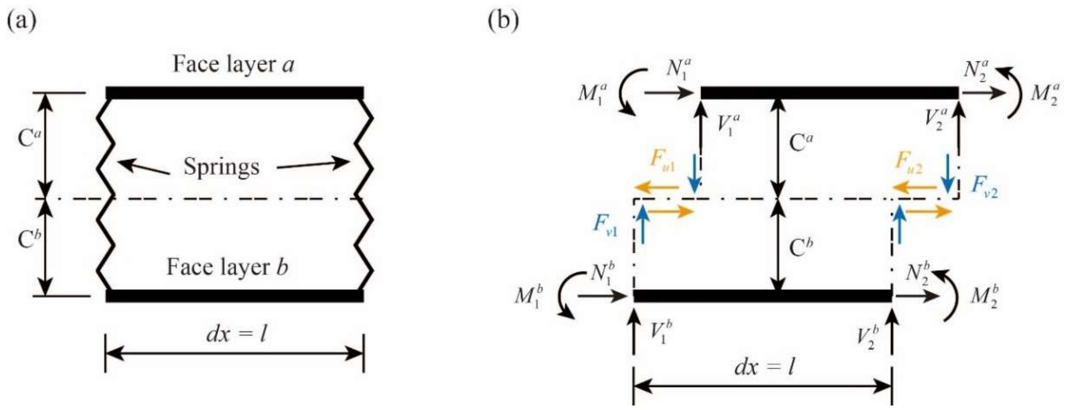

Fig. 3 A composite element with three layers: (a) element components and (b) nodes and force in a deformed element.

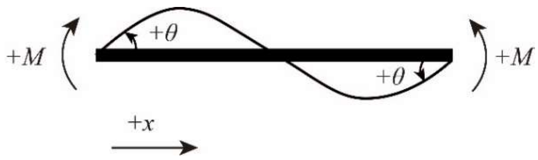

Fig. 4 Sign convention used in the composite element.

The sign convention shown in Fig. 4 was adopted in this study. From the moment equilibrium of the face layer *a*, moment at a distance *x* from node 1 can be written as:

$$M^{a}(x) = -M_{1}^{a} + V_{1}^{a}x + F_{u1}C^{a} - F_{v1}x \tag{2}$$

or as:

$$M^{a}(x) = M_{2}^{a} + V_{2}^{a}(l-x) - F_{u2}C^{a} - F_{v2}(l-x) \tag{3}$$

The force equilibrium equations at nodes 1 and 2 of face layer *a* can be expressed in Eqs. (4) and (5) respectively,

$$N_{1}^{a} - F_{u1} - \frac{(u_{1}^{a} - u_{2}^{a})}{l}E^{a}A^{a} = 0 \tag{4}$$

$$N_{2}^{a} - F_{u2} + \frac{(u_{1}^{a} - u_{2}^{a})}{l}E^{a}A^{a} = 0 \tag{5}$$

The boundary conditions for face layer *a* are:

$$\begin{cases} \left.\dfrac{dv}{dx}\right|_{x=0} = \theta_{1}^{a} \\ v\big|_{x=0} = v_{1}^{a} \\ \left.\dfrac{dv}{dx}\right|_{x=l} = \theta_{2}^{a} \\ v\big|_{x=l} = v_{2}^{a} \end{cases} \tag{6}$$

Similarly, for face layer *b*, the moment at a distance *x* from the node 1 can be expressed as:

$$M^b(x) = -M_1^b + V_1^b x + F_{u1} C_b + F_{v1} x \tag{7}$$

or as:

$$M^b(x) = M_2^b + V_2^b (l - x) - F_{u2} C_b + F_{v2} (l - x) \tag{8}$$

The force equilibrium equations at nodes 1 and 2 of face layer *b* can be expressed in Eqs. (9) and (10) respectively,

$$N_1^b + F_{u1} - \frac{(u_1^b - u_2^b)}{l} E^b A^b = 0 \tag{9}$$

$$N_2^b + F_{u2} + \frac{(u_1^b - u_2^b)}{l} E^b A^b = 0 \tag{10}$$

The boundary conditions for face layer *b* are:

$$\begin{cases} \left.\dfrac{dv}{dx}\right|_{x=0} = \theta_1^b \\ v_{x=0} = v_1^b \\ \left.\dfrac{dv}{dx}\right|_{x=l} = \theta_2^b \\ v\big|_{x=l} = v_2^b \end{cases} \tag{11}$$

According to assumption (c), the face layers are Euler-Bernoulli beams and the moment in face layers *a* and *b* can be written as:

$$M^a = E^a I^a \frac{d^2 y}{dx^2} \tag{12}$$

$$M^b = E^b I^b \frac{d^2 y}{dx^2} \tag{13}$$

Using the stiffness of shear (K_s) and normal (K_n) interlayer springs, the shear forces F_{ui} and normal forces F_{vi} can be calculated as:

$$F_{u1} = K_s \gamma_1 \tag{14}$$

$$F_{u2} = K_s \gamma_2 \tag{15}$$

$$F_{v1} = K_n (v_1^a - v_1^b) \tag{16}$$

$$F_{v2} = K_n (v_2^a - v_2^b) \tag{17}$$

Combining Eqs. (1)-(3), (6), (12), and (14)-(17), the moments and normal forces at face layer *a* can be determined as:

$$M_1^a = K_s C^a (u_1^a - u_1^b + \theta_1^a C^a + \theta_1^b C^b) + \frac{6E^a I^a}{l^2}(v_1^a - v_2^a) + \frac{2E^a I^a}{l}(2\theta_1^a + \theta_2^a) \tag{18}$$

$$M_2^a = K_s C^a (u_2^a - u_2^b + \theta_2^a C^a + \theta_2^b C^b) + \frac{6E^a I^a}{l^2}(v_1^a - v_2^a) + \frac{2E^a I^a}{l}(2\theta_2^a + \theta_1^a) \tag{19}$$

$$V_1^a = \frac{12E^a I^a}{l^3}(v_1^a - v_2^a + \frac{l}{2}\theta_1^a + \frac{l}{2}\theta_2^a) + K_n (v_1^a - v_1^b) \tag{20}$$

$$V_2^a = -\frac{12E^a I^a}{l^3}(v_1^a - v_2^a + \frac{l}{2}\theta_1^a + \frac{l}{2}\theta_2^a) + K_n (v_2^a - v_2^b) \tag{21}$$

Combining Eqs. (1), (4), (5), (14), and (15), the nodal axial forces of face layer *a* can be determined as:

$$N_1^a = (u_1^a - u_2^a)\frac{E^a A^a}{l} + K_s (u_1^a - u_1^b) + K_s (\theta_1^a C^a + \theta_1^b C^b) \tag{22}$$

$$N_2^a = (u_2^a - u_1^a)\frac{E^a A^a}{l} + K_s(u_2^a - u_2^b) + K_s(\theta_2^a C^a + \theta_2^b C^b) \tag{23}$$

Similarly, the moments and normal forces at face layer b can be derived from Eqs. (1), (7), (8), (11), and (13)-(17) as:

$$M_1^b = K_s C^b(u_1^a - u_1^b + \theta_1^a C^a + \theta_1^b C^b) + \frac{6E^b I^b}{l^2}(v_1^b - v_2^b) + \frac{2E^b I^b}{l}(2\theta_1^b + \theta_2^b) \tag{24}$$

$$M_2^b = K_s C^b(u_2^a - u_2^b + C^a\theta_2^a + C^b\theta_2^b) + \frac{6E^b I^b}{l^2}(v_1^b - v_2^b) + \frac{2E^b I^b}{l}(2\theta_2^b + \theta_1^b) \tag{25}$$

$$V_1^b = \frac{12E^b I^b}{l^3}(v_1^b - v_2^b + \frac{l}{2}\theta_1^b + \frac{l}{2}\theta_2^b) - K_n(v_1^a - v_1^b) \tag{26}$$

$$V_2^b = -\frac{12E^b I^b}{l^3}(v_1^b - v_2^b + \frac{l}{2}\theta_1^b + \frac{l}{2}\theta_2^b) - K_n(v_2^a - v_2^b) \tag{27}$$

The nodal axial forces of face layer b can be derived from Eqs. (1), (9), (10), (14), and (15) as:

$$N_1^b = (u_1^b - u_2^b)\frac{E^b A^b}{l} + K_s(u_1^b - u_1^a) - K_s(\theta_1^a C^a + \theta_1^b C^b) \tag{28}$$

$$N_2^b = (u_2^b - u_1^b)\frac{E^b A^b}{l} - K_s(u_2^a - u_2^b) - K_s(\theta_2^a C^a + \theta_2^b C^b) \tag{29}$$

To present the above equations in a general form, element node numbering $2i$-1, $2i$, $2i$+1, and $2i$+2 are introduced for nodes 1b, 1a, 2a, and 2b as shown in Fig. 5.

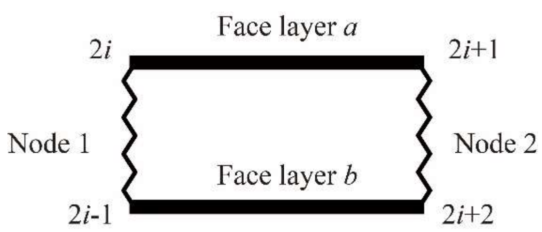

Fig. 5 Node numbering in one composite element.

With the adopted notation for the nodes, a matrix form is summarised for Eqs. (18)-(29) as shown in Eq. (30):

$$\begin{bmatrix} N_{2i-1} \\ V_{2i-1} \\ M_{2i-1} \\ N_{2i} \\ V_{2i} \\ M_{2i} \\ N_{2i+1} \\ V_{2i+1} \\ M_{2i+1} \\ N_{2i+2} \\ V_{2i+2} \\ M_{2i+2} \end{bmatrix} = \begin{bmatrix} N_1^b \\ V_1^b \\ M_1^b \\ N_1^a \\ V_1^a \\ M_1^a \\ N_2^a \\ V_2^a \\ M_2^a \\ N_2^b \\ V_2^b \\ M_2^b \end{bmatrix} = \begin{bmatrix} K_{(2i-1)(2i-1)} & K_{(2i-1)(2i)} & K_{(2i-1)(2i+1)} & K_{(2i-1)(2i+2)} \\ K_{(2i)(2i-1)} & K_{(2i)(2i)} & K_{(2i)(2i+1)} & K_{(2i)(2i+2)} \\ K_{(2i+1)(2i-1)} & K_{(2i+1)(2i)} & K_{(2i+1)(2i+1)} & K_{(2i+1)(2i+2)} \\ K_{(2i+2)(2i-1)} & K_{(2i+2)(2i)} & K_{(2i+2)(2i+1)} & K_{(2i+2)(2i+2)} \end{bmatrix} \begin{bmatrix} u_{2i-1} \\ v_{2i-1} \\ \theta_{2i-1} \\ u_{2i} \\ v_{2i} \\ \theta_{2i} \\ u_{2i+1} \\ v_{2i+1} \\ \theta_{2i+1} \\ u_{2i+2} \\ v_{2i+2} \\ \theta_{2i+2} \end{bmatrix} \tag{30}$$

The components of the stiffness matrix $[K_{mn}]$ (m and n are taken as $2i$-1, $2i$, $2i$+1 or $2i$+2) are as listed in the Appendix.

3. Solution procedure

The previous section presented the formulation of the proposed composite element for a three-layer sandwich beam segment. Then a complete sandwich beam can be discretised into n proposed composite elements, as shown in Fig. 6. n is selected as an odd number so that there is an element at mid-span. An even number of elements would instead introduce a node, and shear spring at the mid-span, complicating the solution procedure. For the current study, node numbering was as shown in Fig. 6, with an element length l=Span/n.

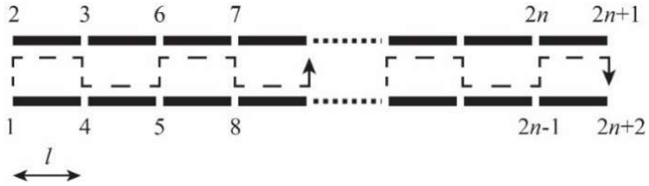

Fig. 6 A discretised sandwich beam with n elements and $2n$+2 nodes.

At the linear stage, the relationship between the displacement $[U]$ and external force $[F]$ of the sandwich panel can be written as:

$$[U]=[K]^{-1}[F] \tag{31}$$

where $[K]$ is the global stiffness matrix, assembled by combining the element stiffness matrices $[K_{mn}]$ from Eq. (30).

When the constituents behave linear elastically, Eq. (31) can be solved directly. However, when the behaviour of the constituents becomes nonlinear, values of $[K_{mn}]$ are no longer constant with different loads, thus a direct solution is not possible. Therefore, a stepwise solution procedure, with updating of $[K_{mn}]$ at each step is proposed to account for nonlinearity of the constituents.

The proposed solution method is presented in Fig. 7 and comprises incremental application of a small load increment $[\Delta F_p]$, with p = 0, 1, 2, 3… and $[\Delta F_0]$ denoted as $[F_0]$. The load increment size should be sufficiently small to ensure a converged modelling result. Further explanation of the solution method is as follows.

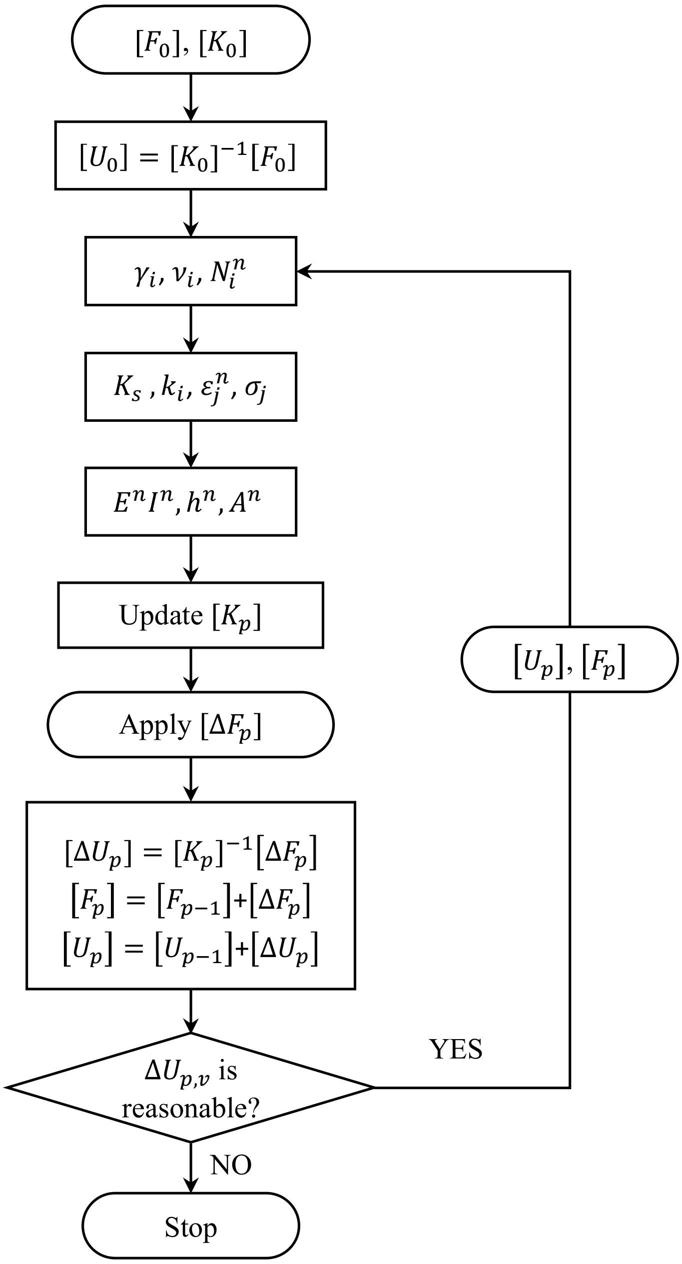

Fig. 7 Nonlinear procedure of the model.

Step 1: The initial stiffness matrix $[K_0]$ is determined using the initial condition of the composite beam using Eq. (30) and Eqs. (A.1)-(A.13). Define $[F_0]$ (small enough to ensure the structure is at linear stage), and then calculate the displacements of the initial $[U_0]$ by Eq. (31).

Step 2: Based on the calculated displacement $[U_{p-1}]$ (p = 1, 2, 3…), the components K_s, h^n, A^n, and $E^n I^n$ in the stiffness matrix $[K_p]$ is updated by following the sub-steps:

i. Calculate the interfacial slip γ_i at the element ends using Eq. (1) with the deformation $[U_{p-1}]$, and then update the shear spring stiffness K_s according to the constitutive relationship of the shear spring.

ii. Determine the strain distribution of each element, at the element mid-length. Strain is evaluated by dividing each face layer into *m* vertical sub-divisions, assuming the neutral axis is at the geometrical centre of the sandwich panel and the strain distributes linearly within each layer as shown in Fig. 8. Resulting strain in each layer was considered to of two parts, strain due to bending and strain due to axial forces. Considering both, axial forces and bending, strain in sub-division *j* of the face layer *n* is calculated as:

$$\varepsilon_j^n = k_{i+1/2} y_j + \frac{\left(N_i^n + N_{i+1}^n\right)}{2A^n E^n} \tag{32}$$

where y_j is the distance to the centre of subdivision *j* from the centroid of the whole section (Fig. 8); N_i^n is the axial force in face layer *n* at node *i* in $[F_{p-1}]$; $k_{i+1/2}$ is the curvature of the element between node *i* and *i*+1, as calculated from the vertical deformation of the element using second order central difference method [42]:

$$k_{i+1/2} = \frac{v_{i-1} - v_i - v_{i+1} + v_{i+2}}{2l^2} \tag{33}$$

where v_i is the vertical displacement of node *i* in $[U_{p-1}]$; *i* is the interested node, *i*-1, *i*+1, and *i*+2 are the adjacent nodes of node *i* in the face layer. For instance, if *i* is node 4 in Fig. 6, *i*-1, *i*+1, and *i*+2 are nodes 1, 2, and 8, respectively.

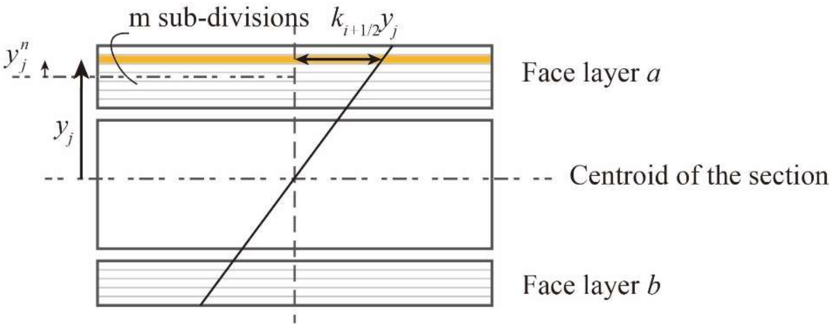

Fig. 8 Strain distribution of the panel due to bending.

iii. Determine the stress profile of the face layers according to the constitutive model of the material, either with linear or nonlinear properties. If the stress σ_j at a sub-division reaches the material strength, that sub-division is deleted, then the face layer height h^n and cross section area A^n are updated.

iv. Calculate the equivalent bending stiffness of each face layer E^nI^n [43], from the obtained stress profile using:

$$E^nI^n = \frac{M_{i+1/2}}{k_{i+1/2}} = \frac{w^n \sum_{j=1}^{m} \left(\sigma_j - \frac{N_i^n + N_{i+1}^n}{2A^n} \right) y_j^n}{k_{i+1/2}} \tag{34}$$

Where $M_{i+1/2}$ is the bending moment in a face layer of the element between node *i* and *i*+1, w^n is the width of the face layer *n*, y_j^n is the distance from the centreline of sub-division *j* to the centreline of the face layer *n* (Fig. 8), and $k_{i+1/2}$ is the curvature of the interested element.

v. Update the components in stiffness matrix $[K_p]$ with the new K_s, A^n, h^n, and E^nI^n.

Step 3: For the applied load increment $[\Delta F_p]$, the increase in deformation $[\Delta U_p]$ can be calculated in Eq. (35), the load $[F_p]$ and deformation $[U_p]$ after the load increment can be calculated by Eqs. (36) and (37):

$$[\Delta U_p]=[K_p]^{-1}[\Delta F_p] \tag{35}$$

$$[F_p]=[F_{p-1}]+[\Delta F_p] \tag{36}$$

$$[U_p]=[U_{p-1}]+[\Delta U_p] \tag{37}$$

Step 4: Repeat steps 2 and 3. Analysis is stopped when the vertical deformation component ($\Delta U_{p,v}$) in $[\Delta U_p]$ become significantly large or changes sign with the applied load increment $[\Delta F_p]$.

4. Model implementation and validation

The above proposed numerical model including the composite element and the solution procedure was implemented by MATLAB software [40]. The proposed model was then verified against the finite element (FE) results using ABAQUS software [44] and experimental results on a series of timber-concrete sandwich panels [13].

4.1. Sandwich beams with linear material properties

First, the verification of the proposed numerical model was carried out, considering only linear elastic materials. Four simply-supported sandwich beams under four-point bending (as shown in Fig. 9) were simulated by both the proposed model and ABAQUS software. The material properties, section sizes, and loading locations of the beams are summarised in Table 1. Beam 1 had two identical face layers, with a 4000mm span and vertical loadings 1300mm away from the supports. Beam 2 was with the same cross section and loading condition as beam 1, while the material property of the top face layer is different. Beam 3 had the same material as beam 2, while the span increased to be 6000mm and the depth of the face layers also increased. Beam 4 had the same material and span as beam 3, but the section width of face layer *b* was smaller than *a*, such that it was similar to a T-shape beam. In all the beams, the interlayer *c* was assumed to be continuous, with a constant thickness of 1 mm and the same width as the narrower face layer. The loads applied on beams 1-4 were 180kN, 100kN, 80kN, and 120kN, respectively.

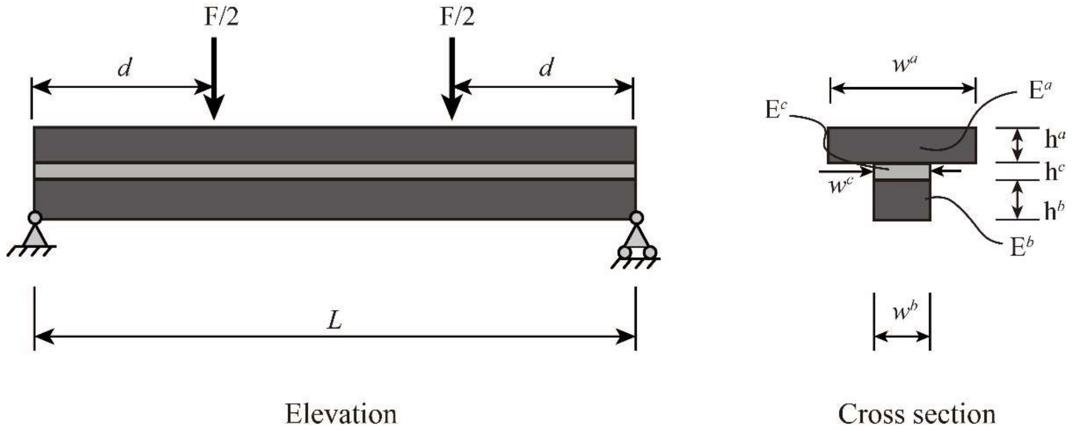

Fig. 9 Beam validation models: loading and geometric parameters.

#	E^a (GPa)	E^b (GPa)	w^a (mm)	w^b (mm)	w^c (mm)	h^a (mm)	h^b (mm)	h^c (mm)	L (mm)	D (mm)	F (kN)
1	200	200	500	500	500	50	50	1	4000	1300	180
2	75	200	500	500	500	50	50	1	4000	1300	100
3	75	200	500	500	500	60	60	1	6000	2000	80
4	75	200	500	200	200	100	100	1	6000	2000	120

Table 1 Details of the four linear sandwich beams.

4.1.1. Details of the finite element model

In the finite element model, the two face layers were modelled with plane stress elements and the interlayer was modelled with cohesive elements [45]. It was assumed that there was no relative slip between the face layers and the interlayer, thus the connection between them was modelled with tie constraints. “Static, general” solver was utilised in the simulation. The material properties as listed in Table 1, both face layers were modelled as isotropic material with a Poisson's ratio of 0.3. The constitutive behaviour of the cohesive element was defined using the uncoupled linear traction-separation law as given in Eq. (38) [45-47].

$$\begin{Bmatrix} t_n \\ t_s \\ t_t \end{Bmatrix} = \begin{bmatrix} E_{nn} & 0 & 0 \\ 0 & E_{ss} & 0 \\ 0 & 0 & E_{tt} \end{bmatrix} \begin{Bmatrix} \delta_n \\ \delta_s \\ \delta_t \end{Bmatrix} \tag{38}$$

where t_n, t_s, and t_t represent the tractions in the normal and two local shear directions respectively; E_{nn}, E_{ss}, and E_{tt} represent the corresponding elastic stiffnesses; and δ_n, δ_s, and δ_t represent the corresponding separations. In this simulation, E_{nn}, E_{ss}, and E_{tt} were taken to be 11.2GPa, 4.31GPa, and 4.31GPa, respectively.

A convergence study was carried out to determine the appropriate mesh size for the ABAQUS models, and the selected element sizes and the minimum element numbers for each sandwich beam are given in Table 2. In beams 1 and 2, a minimum of 200 elements is required to provide reliable results, while in beams 3 and 4, 360 and 300 elements are required respectively.

#	Max. element size, mm (face layers, length×height)	Max. element size, mm (interlayer, length×height)	Min. element number
1 and 2	100×12.5	100×1	200
3	150×15	150×1	360
4	200×20	200×1	300

Table 2 Element size and number of the convergence study in the finite element models.

4.1.2. Details of the proposed model

The properties of face layers *a* and *b* as listed in Table 1 were used in the proposed model. The interlayer shear force is assumed to be taken only by the shear springs at element ends. The shear stiffness of the interlayer spring is determined by the shear modulus and geometry of the interlayer and the element length as, :

$$K_s = \frac{G^c w^c l}{h^c} \tag{39}$$

where h^c and w^c are the depth and width of the interlayer; l is the length of the element; and G^c is the shear modulus of the interlayer, calculated as $G^c = \frac{E^c}{2(1+\nu^c)}$. E^c and ν^c are the elastic modulus and Poisson's ratio of the interlayer, and assumed to be 11.2GPa and 0.3, respectively. For each 100mm length of the interlayer, the shear spring stiffness was 2.15×10^8 N/mm in beams 1-3, and 8.62×10^7 N/mm in beam 4. A stiffness of $K_n=5\times10^{15}$ N/mm was used for the normal spring.

A convergence study showed that for beams 1 and 2, 25 elements (with an element length of approximately 160mm) can provide a converged solution, while for beams 3 and 4, 27 elements (with an element size of approximately 222mm) were required.

4.1.3. Results comparison

The load-displacement curves from the finite element models and the proposed numerical models are compared in Fig. 10. The load-deformation behaviour of all the beams were linear, as expected due to linear elastic material properties used in the models. The stiffness values (calculated as load/deformation) obtained from the load-midspan displacement curves of the FE and proposed models are listed in Table 3. As can be seen from Fig. 10 and Table 3, the FE model and the proposed model agree well with each other for all cases, with a maximum difference in overall stiffness of less than 1.5%. This validates the accuracy of the proposed composite element in predicting the linear elastic behaviour of the sandwich beams.

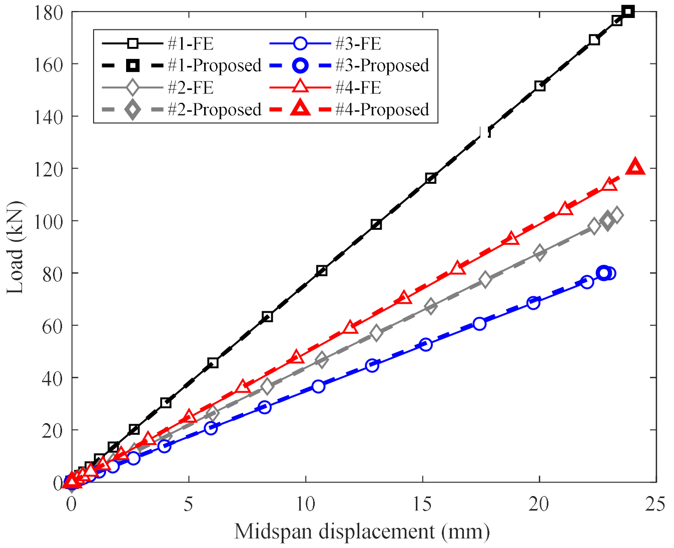

Fig. 10 Load-displacement curves of four linear sandwich beams.

#	FE model (kN/mm)	Proposed model (kN/mm)	Difference (%)
1	7.57	7.57	0
2	4.38	4.36	0.46
3	3.47	3.52	1.44
4	4.93	4.98	1.01

Table 3 Comparison of stiffness of linear sandwich beams.

4.2 Timber-concrete sandwich panel with nonlinear material properties

4.2.1 Details of the specimen

The proposed numerical model (i.e., the composite element and the solution procedure) is used to predict the behaviour of one-way hybrid timber-concrete sandwich panels with a cellular core tested under flexural loading [13]. The investigated sandwich panel is composed of a concrete top layer, a timber bottom layer, and a waffle-shaped core layer between them, as shown in Fig. 11. The core part is composed of longitudinal and transverse plates, connected to each other by integral mechanical joints. The panels, which had a span of 2250mm, were tested under four-point bending with simply-supported boundary conditions. The point loads were applied symmetrically with respect to the panel mid-span and had a spacing of 640mm between them as shown in Fig. 11b. For representation in the proposed model, the concrete and timber layers become face layers *a* and *b*, while the core is modelled as the interlayer *c*. The widths of face layers are $w^a=w^b=600$mm, and the heights are $h^a=50$mm, $h^b=35$mm, and $h^c=110$mm.

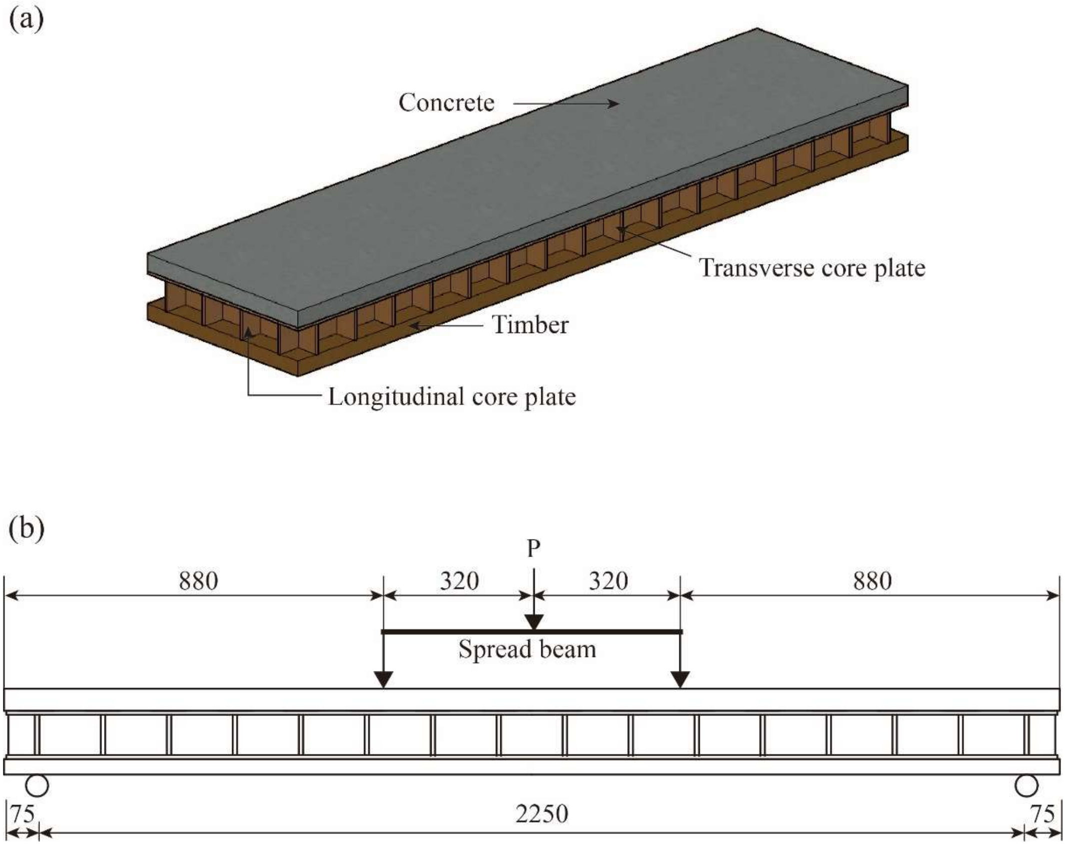

Fig.11 (a) One-way spanning hybrid timber-concrete sandwich panel with a cellular core and (b) loading configuration (unit: mm).

4.2.2 Material properties of the face layers

The concrete layer was modelled using the stress-strain relationship recommended in Eurocode 2 [48]:

$$\sigma = \begin{cases} \varepsilon E_{cm} & \dfrac{f_{ctm}}{E_{cm}} < \varepsilon < 0 \\ \dfrac{1.05E_{cm}\dfrac{\varepsilon}{f_{cm}} - \left(\dfrac{\varepsilon}{\varepsilon_{c1}}\right)^2}{1+\left(1.05E_{cm}\dfrac{\varepsilon_{c1}}{f_{cm}}-2\right)\dfrac{\varepsilon}{\varepsilon_{c1}}} f_{cm} & 0 < \varepsilon < \varepsilon_{cu1} \\ 0 & \text{else} \end{cases} \tag{40}$$

where strain ε is positive when concrete is in compression; f_{cm} is the compressive strength of the concrete; f_{ctm} is the tensile strength of the concrete; E_{cm} is the elastic modulus of the concrete; ε_{c1} is the strain when the stress reaches the compressive strength; and ε_{cu1} is the ultimate compressive strain. For the present study, a concrete strength of f_{cm}=38MPa was adopted, based on material testing as provided in Ref. [13]. Other parameters were determined based on Eurocode 2 as E_{cm}=33GPa, ε_{c1}=2.2%, ε_{cu1}=3.5%, and f_{ctm}=2.9MPa.

The timber layer was modelled as linear elastic until failure. Material properties of timber were obtained according to timber supplier Hyne & Son Pty Ltd [49] and the Australia Standard for timber structures AS1720.1 [50]: an elastic modulus of 13.3GPa, a Poisson's ratio of 0.3, and a characteristic bending strength of 30MPa with 10% coefficient of variation. Although timber is typically an orthotropic material, as in this study only bending of the panel is considered, only the properties parallel to the panel axis and parallel to the grain direction of timber are used for the analysis.

4.2.3 Properties of the interlayer

The sandwich panel core layer is composed of longitudinal and transverse plates in a waffle-type configuration. As the contribution to the shear stiffness from the transverse core plates is much smaller than the longitudinal core plates, it is assumed that the shear stiffness of the core part was provided only by the four longitudinal plates. Based on this assumption, the initial shear stiffness K_s was calculated using a simplified FE model in ABAQUS. Each longitudinal core plate was modelled using S4R 2D plane stress element with orthotropic elastic material properties as provided in Ref. [13]. The translations of the bottom edge were restrained, with the load applied at the top edge of the plate along the x-axis to represent shear action, as shown in Fig. 12. The load and displacement in *x* direction (i.e. horizontal displacement) at the top edge of the core plate was recorded, and the slope of the load-displacement curve was taken as the core shear stiffness of each plate. The total initial shear stiffness K_s of the interlayer was taken as four times of the value of one plate.

A tri-linear shear behaviour as shown in Fig. 13 was used for the interlayer in this study, with the initial stiffness K_s from the ABAQUS model (175.3×10^3N/mm per linear meter). Damage initiation occurs when δ_1=1mm, and the failure happens when shear force drops to F_2=50N at δ_2=1.5mm. Afterwards, the load was assumed to remain at 50N with further increase in slip. Again, according to assumption (d), the vertical spring stiffness of the interlayer was assumed to be 5×10^{10}N/mm.

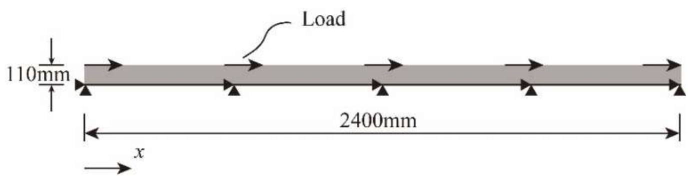

Fig.12 Illustration for calculating the interlayer spring shear stiffness.

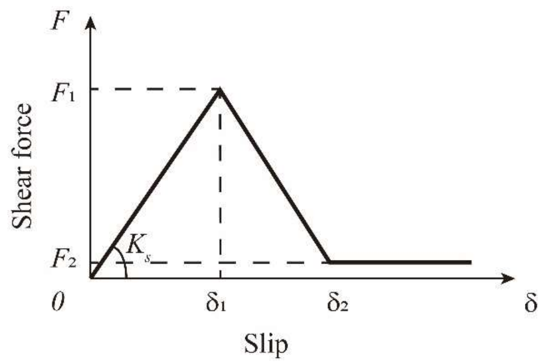

Fig.13 Nonlinear behaviour of the shear spring.

4.2.4 Convergence study of the proposed model

A convergence study was conducted with 9 to 41 elements. An initial vertical load F_{0v}=1kN was first applied to the system, with the vertical loading step then kept constant at ΔF_v=0.1kN. The convergence study results are shown in Fig. 14, with the load-displacement curves shown in Fig. 14a and the predicted loads at the serviceability limit state and ultimate state shown in Fig. 14b. The proposed model provides a consistent load-displacement response for element numbers more than 23, corresponding to an element length l=97.8mm. The prediction obtained with an element number of 23 is therefore chosen to discuss the results.

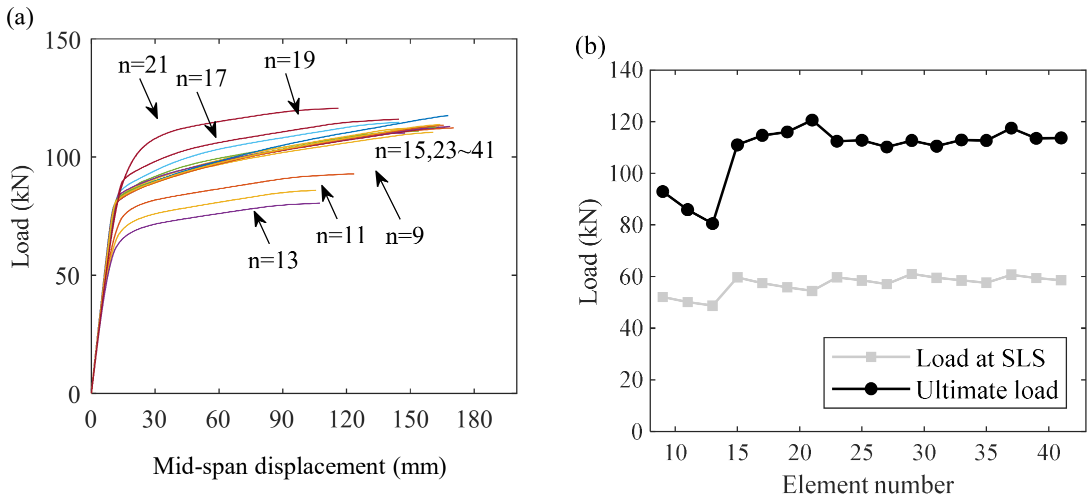

Fig.14 Convergence study results: (a) load-displacement curves, (b) loads at serviceability limit stage and ultimate stage.

4.2.5 Results

The load-displacement curves of the proposed model together with the experimental results of the four specimens tested by the authors [13] are as shown in Fig. 15. The initial stiffness of the curve from the proposed model, up to a load of 40kN, matches the experimental results very well, demonstrating the accuracy of applying the proposed model on the cellular-cored timber-concrete specimens and the calculated core shear stiffness in Section 4.2.3. Besides, the ultimate load predicted by the model was 112.8kN, while the average failure load of the four tested specimens was 113.2kN, with only 0.35% difference.

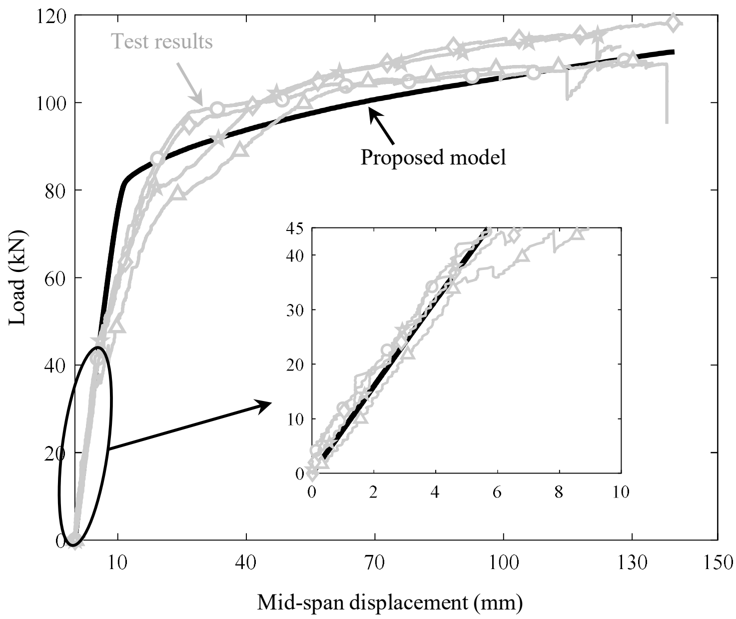

Fig.15 Comparison of predicted and experimental load-displacement curves of hybrid timber-concrete sandwich panels with a cellular core.

At the loading range between 40kN and 80kN, when the experimental curves started to show nonlinearities, the proposed model overestimated the global stiffness. A possible reason for this was that in the proposed model a tri-linear behaviour was assumed for shear springs, so the material behaves linearly before damage initiation. However, the core shear failure was observed to occur gradually in the tested specimens [13], thus the nonlinearity may start from very early stage in the experiments. Nonetheless, the proposed model provided highly accurate prediction for the ultimate load, which depends significantly on the area under the traction-separation curve of the core rather than the shape. Thus, it is clear that in the proposed model, this area matched well with the energy dissipated in the core during the tests. Overall, the proposed model was found to provide a reasonable accuracy for predicting the nonlinear behaviour of the hybrid timber-concrete sandwich panels with a waffle-shaped cellular core.

4.3 Discussion

The proposed composite element was shown to be accurate for prediction of the elastic response of timber-concrete sandwich beams, over a range of material and geometric configurations. The comparison with FE models showed the proposed model to be highly accurate, with a maximum difference in stiffness of less than 1.5%. In terms of the elements used, the proposed method used 25-27 elements while the FE model required 200-360 elements, showing a significant reduction in computational effort.

Results from the proposed methodology agreed well with the nonlinear load-deformation curves from the experimental results of timber-concrete sandwich panels with a waffle-core. This demonstrated the ability of the proposed solution procedure to accurately capture the nonlinear behaviour of the sandwich panels, while keeping the computational effort low. Proposed model can be programmed easily using commercial software packages such as MATLAB, thus can easily be used for design of sandwich panels by practicing engineers.

The shape of the load-deformation curve from the proposed model deviated slightly from the experimental curves, which is believed to be due to the simplified tri-linear traction-separation curve adopted in this study. Work done through shear deformation of the interlayer (represented by the area under the traction-separation curve) significantly affects the load carrying capacity of sandwich panels. Thus, the traction-separation behaviour, numerically derived in the present study, is important for the accurate ultimate load predictions with the proposed model.

Several simplifications were made in the proposed model for calculating the equivalent flexural stiffness of the top and bottom face layers. First, a linear strain distribution was assumed in obtaining the stress distribution through each layer and to update the stiffness matrix. Test results of the timber-concrete sandwich panels used for the comparison showed slightly different curvatures in concrete and timber layers [13], which does not agree with the assumed linear strain distribution. However, as the modelled panels do not compress significantly through thickness, the difference in curvature between top and bottom layers can assumed to be small.

Second, in the current model, discontinuity in strain gradient between the face layers (timber and concrete) was allowed, but discontinuity in strain due to slip between the faces and interlayer (such as the timber and core) was not considered. Slips at the bi-layer interface are not significant compared to the large shear deformation of the interlayer observed in experiments of waffle-core timber-concrete panels, and so the proposed model demonstrated good agreement with experimental curves. However, if the slips at the bi-layer interface become larger, assumed continuous strain behaviour may result in inaccurate strain distributions within each layer, thus resulting in errors.

Third, it is important to note that the solution procedure adopted in this study can only predict accurate results until the ultimate load, and the descending branch of the load displacement curves cannot be predicted. However, since the designers are typically interested only in serviceability and ultimate limit states, the proposed methodology is still useful as a powerful design methodology for sandwich beams.

Finally, the proposed model and solution procedure were validated for the timber-concrete sandwich panels with continuous shear interface, their applicability for sandwich panels with a discretised shear interface, for example with mechanical connectors was not considered as beyond the scope of this study.

5. Conclusions

A simple numerical modelling approach for predicting the flexural behaviour of sandwich beams was presented in this paper. A composite element which considers interlayer slip was proposed. A stepwise solution procedure to account for material nonlinearity was also presented. The developed model is superior to the traditional FE models, with significantly reduced model complexity and computational effort. In addition, proposed model can also be programmed easily using opensource programming languages.

The proposed model was verified first using FE models of sandwich beams with linear elastic material properties and then against experimental results of nonlinear timber-concrete sandwich panels with a waffle-shaped core. Model predictions agreed well with linear elastic FE results, with a maximum difference in stiffness being less than 1.5% whileusing only 25-27 elements, compared to 200-360 elements required for the FE model. Predictions from the proposed numerical model incorporating nonlinear material behaviour also agreed well with the experimental results of the timber-concrete sandwich beams, capturing the ultimate load capacity (with only 0.35% error) and nonlinear behaviours of a complex sandwich beam with only 23 required elements. Central to the accuracy of the proposed approach was the shear traction-separation behaviour of the interlayer, which must be known or obtained using experimental or numerical methods.

The proposed model assumed two face layers to behave as Euler-Bernoulli beams, which is a common assumption made in modelling thin face layers in composite sandwich panels. However, validity of such an assumption may not be true if the face layers are thick, and experience significant transverse deformations. Therefore, further work is necessary to verify the validity of the proposed model for sandwich beams with thick face layers.

Appendix

$$K_{(2i-1)(2i-1)} = \begin{bmatrix} \frac{E^b A^b}{l} + K_s & 0 & -K_s C^b \\ 0 & \frac{12 E^b I^b}{l^3} + K_n & \frac{6 E^b I^b}{l^2} \\ -K_s C^b & \frac{6 E^b I^b}{l^2} & \frac{4 E^b I^b}{l} + K_s \left(C^b\right)^2 \end{bmatrix} \quad \text{(A.1)}$$

$$K_{(2i-1)(2i)}=\begin{bmatrix}-K_s & 0 & -K_sC^a\\ 0 & -K_n & 0\\ K_sC^b & 0 & K_sC^aC^b\end{bmatrix} \tag{A.2}$$

$$K_{(2i-1)(2i+2)}=\begin{bmatrix}-\dfrac{E^bA^b}{l} & 0 & 0\\ 0 & -\dfrac{12E^bI^b}{l^3} & \dfrac{6E^bI^b}{l^2}\\ 0 & -\dfrac{6E^bI^b}{l^2} & \dfrac{2E^bI^b}{l}\end{bmatrix} \tag{A.3}$$

$$K_{(2i)(2i-1)}=\begin{bmatrix}-K_s & 0 & K_sC^b\\ 0 & -K_n & 0\\ -K_sC^a & 0 & K_sC^aC^b\end{bmatrix} \tag{A.4}$$

$$K_{(2i)(2i)}=\begin{bmatrix}\dfrac{E^aA^a}{l}+K_s & 0 & K_sC^a\\ 0 & \dfrac{12E^aI^a}{l^3}+K_n & \dfrac{6E^aI^a}{l^2}\\ K_sC^a & \dfrac{6E^aI^a}{l^2} & \dfrac{4E^aI^a}{l}+K_s\left(C^a\right)^2\end{bmatrix} \tag{A.5}$$

$$K_{(2i)(2i+1)}=\begin{bmatrix}-\dfrac{E^aA^a}{l} & 0 & 0\\ 0 & -\dfrac{12E^aI^a}{l^3} & \dfrac{6E^aI^a}{l^2}\\ 0 & -\dfrac{6E^aI^a}{l^2} & \dfrac{2E^aI^a}{l}\end{bmatrix} \tag{A.6}$$

$$K_{(2i+1)(2i)}=\begin{bmatrix}-\dfrac{E^aA^a}{l} & 0 & 0\\ 0 & -\dfrac{12E^aI^a}{l^3} & -\dfrac{6E^aI^a}{l^2}\\ 0 & \dfrac{6E^aI^a}{l^2} & \dfrac{2E^aI^a}{l}\end{bmatrix} \tag{A.7}$$

$$K_{(2i+1)(2i+1)}=\begin{bmatrix}\dfrac{E^aA^a}{l}+K_s & 0 & K_sC^a\\ 0 & \dfrac{12E^aI^a}{l^3}+K_n & -\dfrac{6E^aI^a}{l^2}\\ K_sC_a & -\dfrac{6E^aI^a}{l^2} & \dfrac{4E^aI^a}{l}+K_s\left(C^a\right)^2\end{bmatrix} \tag{A.8}$$

$$K_{(2i+1)(2i+2)}=\begin{bmatrix}-K_s & 0 & K_sC^b\\ 0 & -K_n & 0\\ -K_sC^a & 0 & K_sC^aC^b\end{bmatrix} \tag{A.9}$$

$$K_{(2i+2)(2i-1)}=\begin{bmatrix}-\dfrac{E^bA^b}{l} & 0 & 0\\ 0 & -\dfrac{12E^bI^b}{l^3} & -\dfrac{6E^bI^b}{l^2}\\ 0 & \dfrac{6E^bI^b}{l^2} & \dfrac{2E^bI^b}{l}\end{bmatrix} \tag{A.10}$$

$$K_{(2i+2)(2i+1)}=\begin{bmatrix}-K_s & 0 & -K_sC^a\\ 0 & -K_n & 0\\ K_sC^b & 0 & K_sC^aC^b\end{bmatrix} \tag{A.11}$$

$$K_{(2i+2)(2i+2)}=\begin{bmatrix}\dfrac{E^bA^b}{l}+K_s & 0 & K_sC^a\\ 0 & \dfrac{12E^aI^a}{l^3}+K_n & -\dfrac{6E^bI^b}{l^2}\\ K_sC^a & -\dfrac{6E^bI^b}{l^2} & \dfrac{4E^bI^b}{l}+K_s(C^b)^2\end{bmatrix} \tag{A.12}$$

$$K_{(2i-1)(2i+1)}=K_{(2i)(2i+2)}=K_{(2i+1)(2i-1)}=K_{(2i+2)(2i)}=\left[0\right]_{3\times3} \tag{A.13}$$

Notations

a	upper face layer of the sandwich panel
A^n	cross section area of face layer n, n is a or b
b	lower face layer of the sandwich panel
c	interlayer of the sandwich panel
C^n	distance from the centreline of face layer n to the centreline of interlayer, n is a or b
d	distance from loading points to supports in a beam under four-point bending
E_{cm}	elastic modulus of concrete
E^n	elastic modulus of the material in layer n, n is a, b or c
E_{nn}	elastic stiffness at the normal direction of the interface
E_{ss}/E_{tt}	elastic stiffness at the shear direction of the interface
f_{cm}	compressive strength of concrete
f_{ctm}	tensile strength of concrete

F_1	strength of interlayer shear spring
F_2	shear force of the interlayer when the shear deformation is large
F_{ui}	shear force at node *i* in the interlayer
F_{vi}	normal force at node *i* in the interlayer
$[F]$	external force vector
$[F_p]$	external force vector at load step *p*
G^c	shear modulus of the interlayer material
h^n	section height of face layer or interlayer *n*, *n* is *a*, *b* or *c*
I^n	second moment of area of face layer *n*, *n* is *a* or *b*
$k_{i+1/2}$	curvature of the element between node *i* and *i+1*
K_s	stiffness of the shear spring
K_n	stiffness of the normal spring
K_{mn}	a component relating to nodes *m* and *n* in the proposed stiffness matrix
$[K_p]$	global stiffness matrix of the panel at load step *p*
l	length of the composite element
L	span of the sandwich beam
m	number of sub-divisions in a face layer
M_i^n	bending moment in face layer *n* at point *i*, *n* is *a* or *b*
N_i^n	axial force in face layer *n* at point *i*, *n* is *a* or *b*
t_n	traction in normal direction of the interface
t_s/t_t	traction in shear direction of the interface
u_i^n	deformation along x-axis in face layer *n* at node *i*, *n* is *a* or *b*
$[U_p]$	deformation vector after load step *p*
v_i^n	vertical deformation in face layer *n* at node *i*, *n* is *a* or *b*
V_i^n	shear force in face layer *n* at node *i*, *n* is *a* or *b*
w^n	width of the face layer or interlayer *n*, *n* is *a*, *b* or *c*
y_j	distance from the centreline of sub-division *j* to the geometrical centre of the sandwich beam
y_j^n	distance from the centreline of sub-division *j* to the centreline of face layer *n*, *n* is *a* or *b*
ε_j^n	axial strain of sub-division *j* in face layer *n*, *n* is *a* or *b*
ε_{c1}	concrete strain at the compressive strength
ε_{cu1}	concrete ultimate compressive strain
ε_n	separation at the normal direction of the interface

$\varepsilon_t / \varepsilon_s$	separation at the shear direction of the interface
δ_1	shear deformation at the maximum shear force
δ_2	shear deformation in the interlayer when it fails
θ_i^n	rotation of face layer *n* at node *i*, *n* is *a* or *b*
γ_i	relative slip between two face layers
ν^f	Poisson's ratio of the interlayer material

References

[1] Yeoh D, Fragiacomo M, De Franceschi M, Heng Boon K. State of the art on timber-concrete composite structures: literature review. J Struct Eng 2011;137:1085-95. https://doi.org/10.1061/(ASCE)ST.1943-541X.0000353.

[2] Ceccotti A. Composite concrete-timber structures. Prog Struct Eng Mater 2002;4:264-75. http://dx.doi.org/10.1002/pse.126.

[3] Sipari H. Architektonishe gestaltunggsmöglichkeiten dank doppelkopfschraub. STZ 1985;Nr. 10.

[4] Van der Linden MLR. Timber-concrete composite beams. Heron 1999;44:215-39.

[5] Djoubissie DD, Messan A, Fournely E, Bouchaïr A. Experimental study of the mechanical behavior of timber-concrete shear connections with threaded reinforcing bars. Eng Struct 2018;172:997-1010. https://doi.org/10.1016/j.engstruct.2018.06.084.

[6] Boccadoro L, Frangi A. Experimental analysis of the structural behavior of timber-concrete composite slabs made of beech-laminated veneer lumber. J Perform Constr Facil 2014;28:A4014006. https://doi.org/10.1061/(ASCE)CF.1943-5509.0000552.

[7] Boccadoro L, Zweidler S, Steiger R, Frangi A. Bending tests on timber-concrete composite members made of beech laminated veneer lumber with notched connection. Eng Struct 2017;132:14-28. https://doi.org/10.1016/j.engstruct.2016.11.029.

[8] Gutkowski RM, Brown K, Shigidi A, Natterer J. Laboratory tests of composite wood-concrete beams. Constr Build Mater 2008;22:1059-66. http://dx.doi.org/10.1016/j.conbuildmat.2007.03.013.

[9] Brunner M, Romer M, Schnüriger M. Timber-concrete-composite with an adhesive connector (wet on wet process). Mater Struct 2006;40:119-26. https://doi.org/10.1617/s11527-006-9154-4.

[10] Zhu W, Yang H, Liu W, Shi B, Ling Z, Tao H. Experimental investigation on innovative connections for timber–concrete composite systems. Constr Build Mater 2019;207:345-56. https://doi.org/10.1016/j.conbuildmat.2019.02.079.

[11] Otero-Chans D, Estévez-Cimadevila J, Suárez-Riestra F, Martín-Gutiérrez E. Experimental analysis of glued-in steel plates used as shear connectors in timber-concrete-composites. Eng Struct 2018;170:1-10. https://doi.org/10.1016/j.engstruct.2018.05.062.

[12] Ou Y, Gattas JM, Fernando D, Torero JL. Experimental investigation of a timber-concrete floor panel system with a hybrid glass fibre reinforced polymer-timber corrugated core. Eng Struct 2020;203:109832. https://doi.org/10.1016/j.engstruct.2019.109832.

[13] Ou Y, Fernando D, Gattas JM. Experimental investigation of a novel concrete-timber floor panel system with digitally fabricated FRP-timber hollow core component. Constr Build Mater 2019;227:116667. https://doi.org/10.1016/j.conbuildmat.2019.08.048.

[14] Dey V, Zani G, Colombo M, Di Prisco M, Mobasher B. Flexural impact response of textile-reinforced aerated concrete sandwich panels. Mater Des 2015;86:187-97. https://doi.org/10.1016/j.matdes.2015.07.004.
[15] Manalo A, Aravinthan T, Fam A, Benmokrane B. State-of-the-art review on FRP sandwich systems for lightweight civil infrastructure. J Compos Constr 2016:04016068. https://doi.org/10.1061/(ASCE)CC.1943-5614.0000729.
[16] Liu Q, Du W, Uddin N, Zhou Z. Flexural behaviors of concrete/EPS-foam/glass-fiber composite sandwich panel. Adv Mater Sci Eng 2018;2018:5286757. https://doi.org/10.1155/2018/5286757.
[17] Edgars L, Kaspars Z, Kaspars K. Structural performance of wood based sandwich panels in four point bending. Procedia Eng 2017;172:628-33. https://doi.org/10.1016/j.proeng.2017.02.073.
[18] Vervloet J, Van Itterbeeck P, Verbruggen S, El Kadi M, De Munck M, Wastiels J et al. Experimental investigation of the buckling behaviour of textile reinforced cement sandwich panels with varying face thickness using digital image correlation. Constr Build Mater 2019;194:24-31. https://doi.org/10.1016/j.conbuildmat.2018.11.015.
[19] Awad ZK, Aravinthan T, Zhuge Y. Experimental and numerical analysis of an innovative GFRP sandwich floor panel under point load. Eng Struct 2012;41:126-35. https://doi.org/10.1016/j.engstruct.2012.03.023.
[20] Chen W, Si J. A model of composite laminated beam based on the global–local theory and new modified couple-stress theory. Compos Struct 2013;103:99-107. https://doi.org/10.1016/j.compstruct.2013.03.021.
[21] Frostig Y, Baruch M, Vilnay O, Sheinman I. High-order theory for sandwich-beam behavior with transversely flexible core. J Eng Mech 1992;118:1026-43. https://doi.org/10.1061/(ASCE)0733-9399(1992)118:5(1026).
[22] Goswami S, Becker W. Analysis of sandwich plates with compressible core using layerwise refined plate theory and interface stress continuity. J Compos Mater 2016;50:201-17. https://doi.org/10.1177/0021998315572929.
[23] Li R, Kardomateas GA. Nonlinear high-order core theory for sandwich plates with orthotropic phases. AIAA J 2008;46:2926-34. https://doi.org/10.2514/1.37430.
[24] Phan CN, Frostig Y, Kardomateas GA. Analysis of sandwich beams with a compliant core and with in-plane rigidity-extended high-order sandwich panel theory versus elasticity. J Appl Mech 2012;79. https://doi.org/10.1115/1.4005550.
[25] Battini J-M, Nguyen Q-H, Hjiaj M. Non-linear finite element analysis of composite beams with interlayer slips. Comput Struct 2009;87:904-12. https://doi.org/10.1016/j.compstruc.2009.04.002.
[26] Khorsandnia N, Valipour H, Bradford M. Deconstructable timber-concrete composite beams with panelised slabs: Finite element analysis. Constr Build Mater 2018;163:798-811. https://doi.org/10.1016/j.conbuildmat.2017.12.169.
[27] Gutkowski RM, Balogh J, To LG. Finite-element modeling of short-term field response of composite wood-concrete floors/decks. J Struct Eng 2010;136:707-14. https://doi.org/10.1061/(ASCE)ST.1943-541X.0000117.
[28] Valipour HR, Bradford MA. A steel-concrete composite beam element with material nonlinearities and partial shear interaction. Finite Elem Anal Des 2009;45:966-72. https://doi.org/10.1016/j.finel.2009.09.011.
[29] Faella C, Martinelli E, Nigro E. Steel and concrete composite beams with flexible shear connection:“exact” analytical expression of the stiffness matrix and applications. Comput Struct 2002;80:1001-9. https://doi.org/10.1016/S0045-7949(02)00038-X.

[30] Lin J-P, Wang G, Bao G, Xu R. Stiffness matrix for the analysis and design of partial-interaction composite beams. Constr Build Mater 2017;156:761-72. https://doi.org/10.1016/j.conbuildmat.2017.08.154.
[31] Valipour H, Khorsandnia N, Crews K, Palermo A. Numerical modelling of timber/timber-concrete composite frames with ductile jointed connection. Adv Struct Eng 2016;19:299-313. https://doi.org/10.1177/1369433215624600.
[32] Akgöz B, Civalek Ö. A microstructure-dependent sinusoidal plate model based on the strain gradient elasticity theory. AcMec 2015;226:2277-94. https://doi.org/10.1007/s00707-015-1308-4.
[33] Jalaei MH, Civalekb Ö. On dynamic instability of magnetically embedded viscoelastic porous FG nanobeam. IJES 2019;143:14-32. https://doi.org/10.1016/j.ijengsci.2019.06.013.
[34] Santos HAFA, Silberschmidt VV. Hybrid equilibrium finite element formulation for composite beams with partial interaction. Compos Struct 2014;108:646-56. https://doi.org/10.1016/j.compstruct.2013.09.062.
[35] Auclair SC, Sorelli L, Salenikovich A. Simplified nonlinear model for timber-concrete composite beams. Int J Mech Sci 2016;117:30-42. https://doi.org/10.1016/j.ijmecsci.2016.07.019.
[36] European Commitee for Standardization CEN. EN 26891 Timber structures- joints made with mechanical fasteners-general principles for the determination of strength and deformation characteristics. 1991.
[37] Teng JG, Fernando D, Yu T. Finite element modelling of debonding failures in steel beams flexurally strengthened with CFRP laminates. Eng Struct 2015;86:213-24. https://doi.org/10.1016/j.engstruct.2015.01.003.
[38] Focacci F, Foraboschi P, De Stefano M. Composite beam generally connected: analytical model. Compos Struct 2015;133:1237-48. https://doi.org/10.1016/j.compstruct.2015.07.044.
[39] Kier Z. Modeling 3D fiber reinforced foam core sandwich structures using a multi-scale finite element approach. Ann Arbor, MI, United States: University of Michigan; 2015.
[40] MathWorks I. MATLAB. R2018a. Natick, Massachusetts, United States2018.
[41] Python Software Foundation. Python. 3.9 ed2020.
[42] Chung T. Derivation of Finite Difference Equations. Computational Fluid Dynamics. Cambridge: Cambridge University Press; 2010. p. 45-62.
[43] Hibbeler RC. Deflection of beams and shafts. Mech Mater. 8th ed: Pearson Prentice Hall; 2011.
[44] Systèmes D. ABAQUS CAE. Providence, Rhode Island, United States2014.
[45] Systèmes D. Abaqus analysis user's guide (6.13). Abaqus 613. Providence, Rhode Island, United States: Simulia Corp; 2014.
[46] Fernando ND. Bond behaviour and debonding failures in CFRP-strengthened steel members. Hong Kong: The Hong Kong Polytechnic University; 2010.
[47] De Lorenzis L, Zavarise G. Modeling of mixed-mode debonding in the peel test applied to superficial reinforcements. Int J Solids Struct 2008;45:5419-36. https://doi.org/10.1016/j.ijsolstr.2008.05.024.
[48] Cen. Eurocode 2: design of concrete structures. Part 1-1: general rules and rules for buildings. London, UK: British Standards Institution; 2004.
[49] Hyne, Son Pty L. HYNE LGL mechanical properties. 2018.
[50] AS 1720.1. Timber structures part 1: design methods. Standards Australia Limited; 2010.